Food Science of Animal Products

Research Article

Effects of biopolymer ratio and pH value on the complex formation between whey protein isolates and soluble *Auricularia auricular* polysaccharides

Xiuliang Li[1,2,3], Yang Su[1,2], Xiaoyun Han[1,2,4], Qixin Yan[1,2], Qingshen Sun[1,2,4] ✉

[1] *Engineering Research Center of Agricultural Microbiology Technology, Ministry of Education, Heilongjiang University, Harbin 150500, China*
[2] *Jiaxiang Research Academy of Industrial Technology, Jining 272400, China*
[3] *Key Laboratory of Molecular Biology, College of Heilongjiang Province, School of Life Sciences, Heilongjiang University, Harbin 150080, China*
[4] *Key Laboratory of Microbiology, College of Heilongjiang Province, School of Life Sciences, Heilongjiang University, Harbin 150080, China*
✉Address correspondence to Qingshen Sun, kejiansqs@163.com; sunqingshen@hlju.edu.cn

Received: December 12, 2022; Revised: January 3, 2023; Accepted: January 25, 2023

Abstract: Biopolymer complexes fabricated by proteins and neutral polysaccharides have some specific and innovative functionalities. A better understanding of the interactions among these biopolymers might provide new insight into the applications of the complexes. Therefore, this study aimed to investigate the structural characteristics and molecular interaction mechanisms of whey protein isolates (WPI) and *Auricularia auricular* polysaccharides (APs). The turbidity analysis confirmed that the pH value and mixing ratio of the two polymers had strong effects on the formation of the APs-WPI complexes. All dispersions formed soluble complexes at approximately pH = 6.0 (pH_c). APs-WPI self-assembles exhibited physically cross-linked networks under higher APs proportions, while they formed spherical complexes at higher WPI ratios. The addition of APs could alter the secondary structure of WPI, and the most noticeable changes were located in the regions of β-sheet and β-turn as confirmed by circular dichroism (CD) analysis. A molecular docking study showed that the amino acid residues of β-lactoglobulin complexed with the –COOH and –OH groups of APs. Hydrogen bonds and hydrophobic interactions, which were nonbonding contributions, played a key role in the formation of the APs-WPI complex. This study provided a basis for the development and application of APs in WPI-based beverages.

Keywords: whey protein isolate; *Auricularia auricular* polysaccharides; interaction; docking

Citation: X. L. Li, Y. Su, X. Y. Han, et al., Effects of biopolymer ratio and pH value on the complex formation between whey protein isolates and soluble *Auricularia auricular* polysaccharides, Food Sci. Anim. Prod. 1 (2023) 9240004. https://doi.org/10.26599/FSAP.2023.9240004.

1 Introduction

The interactions between polysaccharides and proteins endow the complexes with wide applications, such as maintaining food quality and endowing food with specialized functionalities [1]. In aqueous systems, proteins and polysaccharides can form complex aggregates through noncovalent interactions, such as electrostatic adsorption, hydrogen bonding and hydrophobic interactions [2], which are affected by the physicochemical characteristics (e.g., charge density and molar mass), concentration and ratio of polymers, and the solution conditions (e.g., pH value, ionic strength, and temperature). The aqueous pH value and the ratio of protein and polysaccharides are important parameters affecting the formation of protein-polysaccharide complexes. Studies have shown that complex aggregates have better functional activities than individual proteins or polysaccharides [3–5] and have been widely used in stabilizing emulsions, encapsulating active components, improving protein stability, and developing new composite materials [6–9].

Whey protein isolate (WPI) has been widely used to develop various protein-rich beverages due to its high nutritional value, commercial availability, and low cost. WPI mainly consists of β-lactoglobulin (β-Lg), α-lactalbumin (α-La), lactoperoxidase, lactoferrin, and bovine serum albumin (BSA) [10]. Protein-rich beverages are usually formulated around pH 4.0–6.0 [11]. However, WPI is sensitive to solution pH value and suffers from poor stability (aggregation and precipitation) near the isoelectric point (pI), which limits its use in the production of beverages [12]. Therefore, reducing the aggregation and precipitation of WPI at acidic pH value is significant for developing acidic protein beverages. There are three approaches to improve protein solubility. A method called "physical modification" improves protein stability by physical methods, such as pH value, heat treatment and ultrasound. A previous study confirmed that pH 2-shifting treatment (3 h) combined with ultrasound could improve the emulsion stability of WPI [13]. Another method is by bioengineering technology, such as turning WPI into whey isolated protein fibrils [14] or developing a nanoscale delivery system [15]. These methods require many steps, which may be a barrier in the application of WPI. The final way is to add a stabilizer, which is an environmentally friendly and simple. For example, polysaccharides can be used as stabilizers of

© Beijing Academy of Food Sciences 2023. Food Science of Animal Products published by Tsinghua University Press. This is an open access article under the CC BY-NC-ND license (http://creativecommons.org/licenses/by-nc-nd/4.0/).

WPI by forming protein-polysaccharide complexes [9, 16], which can improve the emulsion stability of WPI and polysaccharides, such as *Tremella fuciformis* polysaccharide [12], xanthan gum (XG) [17], and pectin [18].

In recent years, the interaction behaviors between protein and commercial polysaccharides such as pectin, xanthan and carrageenan systems have been studied [19–21]. *Auricularia auricula* polysaccharides (APs) mainly contain *β-D*-glucan (Figure 1) [22, 23]. Polysaccharides with high molecular weight (M_W) can increase viscosity of acidified milk drinks, therefore, contributing to their stability [12, 24]. APs show a M_W of approximately 2.5×10^3 kDa, being a high M_W polysaccharide [22]. Meanwhile, APs exhibit many biological activities (antidiabetic, anticoagulation, antitumor and antioxidant), and excellent thermal stability [25, 26]. The rheological results showed that the APs aqueous solution had higher viscosity than xanthan, a pronounced thickening agent [23]. APs can interact with a variety of proteins including WPI and can relieve astringency of the WPI solution induced in acidic pH value [27], thereby improving the WPI stability [28].

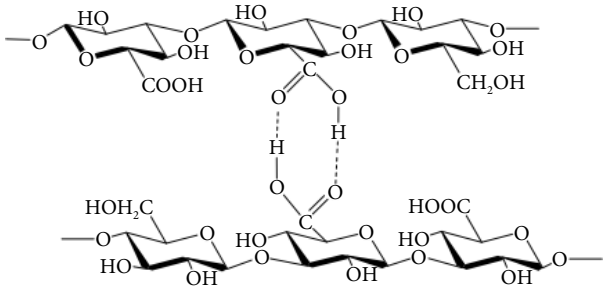


Figure 1 Chemical structure of APs.

The current strategies to study the interactions between WPI and polysaccharides under different pH values include circular dichroism (CD), X-ray diffraction (XRD), atomic force microscopy (AFM), and Fourier transform infrared spectroscopy (FTIR) analysis. Solution turbidity is closely related to the light scattering of dissolved particles. It has also been used as an indicator of the interaction behavior of protein-polysaccharide systems [29]. FTIR could be used to indicate interaction force in the complex and identify the interaction mechanism between APs and WPI. CD spectra were used to characterize the protein secondary structure changes associated with the binding of APs to WPI. AFM, a type of scanning probe microscopy, is a powerful technology to visualize biopolymers, such as polysaccharides and proteins, up to a single molecular level in "near-native" conditions. XRD analyses were performed to obtain crystal structures. The size of the particle can be assessed in terms of its stability in the solution system [28, 30–33]. Furthermore, molecular docking can directly reveal the interactions between two atoms or molecules, which is, therefore, widely used to provide microscopic insights, such as binding sites, interaction types, and structural changes [34–36].

To date, little is known about how the interactions between APs and WPI are realized. As *Auricularia auricula* is the main fungus cultivated in China, the in-depth exploitation of *Auricularia auricula* is necessary. APs have been extracted and used in different forms. Little is known about the effects of APs on WPI stability. Therefore, in this study, the interaction mechanism between APs and WPI was explored to provide a theoretical basis for the application of APs in WPI-based beverages.

2 Materials and methods

2.1 Materials

Senwang *Auricularia auricular* was supplied by Greater Khingan (Heilongjiang, China). Commercial whey protein isolates (water 7%, protein 80%, carbohydrate 3%, total fat 6%, and ash 4%) were supplied by Shanghai Yuanye Bio-technology Co., Ltd. (Shanghai, China).

2.2 Extraction and component analysis of APs

APs were extracted using previously described methods [37]. Briefly, dry *Auricularia auricula* powder (10 g) was immersed in 1.6 L of 1% (*m*/*V*) sodium hydroxide solution at 80 °C for 3 h. Then, the sample was centrifuged at 6 789 × *g* for 10 min. The supernatant was precipitated with 95% ethanol (1:4, *V*/*V*) at 4 °C overnight and centrifuged at 6 789 × *g* for 10 min. The precipitates were resuspended in distilled water and lyophilized to obtain the APs. The polysaccharide and protein contents of the extracted products were determined by the phenol-sulfuric method and Bradford's method, respectively [25]. The contents of uronic acids and total phenolic compounds were determined using the carbazole sulfuric acid method [38] and the Folin-Ciocalteu method [39], respectively.

2.3 Preparation of the APs-WPI solution

APs (1%) stock dispersion (*m*/*m*) and 4% WPI stock dispersion (*m*/*m*) were prepared by dissolving APs and WPI in deionized water overnight at 4 °C, which were adjusted to pH 7.0. The APs stock dispersion was then centrifuged at 6 789 × *g* for 15 min to separate the supernatant. The binary mixtures of APs and WPI at different ratios (at a total concentration of 0.2%) were prepared by mixing the two solutions under agitation for 2 h at room temperature followed by pH value adjustment [29].

2.4 Turbidimetric analysis

The pH-dependent turbidity was measured against a wavelength of 600 nm using a 752 ultraviolet (UV)-visible spectrophotometer (Jinghua Instruments, China) calibrated with ultrapure water to 100% transmittance (%T). Turbidity was defined as 100%T. The pH value of 0.2% APs-WPI solutions (*m*/*m*) was adjusted using 0.1 mol/L HCl under stirring and monitored by a digital pH meter. Then, the samples were vortexed for 5–8 s, followed by quiescent storage at 4 °C for 48 h. Measurements of solution turbidity were performed in triplicates at room temperature [40].

2.5 Structural characterization of the APs-WPI powder

The freeze-dried powders of the APs-WPI solution at pH_{opt} (the maximum soluble complex formation pH) and pH_c (the start of soluble complex formation or tangent lines on either side of inflection points at pH higher than pH_{opt}) were subjected to the following analysis [29].

Particle size analysis of WPI and APs-WPI samples was conducted using a laser diffraction particle size analyzer (BT-9300, Dandong Baite Instrument Co., Ltd.) at pH_{opt}. FTIR analysis was conducted by mixing the samples with potassium bromide to obtain pellets for FTIR detection. FTIR spectra were recorded at wavenumbers of 400–4 000 cm^{-1} using Frontier Mid-IR FTIR (PE, USA). XRD spectra for the APs, WPI, and APs-WPI were directly recorded through powder XRD analysis using a Bruker D8 ADVANCE A25X (Bruker, Germany) equipped with Cu-Kα_1 radiation (λ = 0.154 18 nm) as the X-ray source (40 kV, 10 mA) in the 2θ range of 10°–80°.

2.6 AFM observations

The APs-WPI solutions at different ratios were adjusted to pH_{opt} under magnetic agitation, and then the images of the different ratios of complexes were revealed by AFM. AFM morphology was obtained by scanning samples on a Nanoscope IIIa Multi-Mode AFM (DI, USA). One microliter of soluble complex solution (diluted 400 × with deionized water) was dripped onto a mica surface at room temperature for 24 h. Tapping mode was used for collecting the AFM images.

2.7 CD analysis

WPI and different ratios of APs-WPI at pH_c and pH_{opt} solution samples were diluted to 0.1 mg/mL and measured by a CD spectrophotometer (V100, Applied Photophysics, UK). The CD spectral tests were conducted under a nitrogen atmosphere at room temperature using a quartz cell with a 1 cm path. Absorption spectra of the above samples were recorded between 190 and 260 nm using the following instrumental parameters: bandwidth of 1.00 nm and scanning speed of 20 nm/min. Each spectrum was obtained in triplicate. Data analysis was performed using DichroWeb to calculate the protein secondary structure.

2.8 Molecular docking

The SMINA software was used as a molecular docking tool to investigate the binding processes between *β*-glucan and WPI. In the docking experiments, structures of *β*-Lg, *α*-La, lactoperoxidase, lactoferrin, and BSA were extracted from the PDB database, with the PDB codes 5IO5, 1HFY, 3GC1, 1B1X, and 4F5S, respectively. The chemical structures of *β*-glucan (CID: 439262) were obtained from the PubChem database. The Mol2 files were produced by the RDKit software package to energy minimization and add polar hydrogen. PDBQT files of *β*-glucan and WPI were generated from traditional PDB files by Smina. The best-scoring mode was judged by Vina from nine results and analyzed by PyMol software. Table 1 showed the docking parameters used in this study.

Table 1 Presentation of docking parameters.

PDB ID	*X*-center	*Y*-center	*Z*-center
1B1X	34.563	12.278	22.073
1HFY	9.146	11.478	10.650
3GC1	7.513	−0.601	22.046
4F5S	34.888	23.988	98.761
5IO5	22.237	61.576	22.504

2.9 Statistical analysis

All of the measurements were conducted in triplicate, and the data are presented as the mean ± standard deviation. Statistical analysis of the data was performed using One-Way ANOVA in Origin Pro 8 software to determine the statistical significance at the $P < 0.05$ level.

3 Results and discussion

3.1 The chemical composition of APs and effect of pH value on WPI-APs complex behavior

The APs used in this study contained a total polysaccharide content of 82.17%, uronic acid content of 6.98%, polyphenol content of 7.07%, and no protein detected.

The turbidity measurement has long been applied to identify the boundary pH value of phase behaviors based on optical properties at the mesoscale under low biopolymer concentrations [41]. Figure 2 showed the turbidity of WPI, APs, and their mixtures (with different ratios, *m*/*m*) over pH 2.0–7.0. The absorbance values of the APs dispersion remained constant over a wide range of pH values, indicating that the APs had stable solubility over acidic and neutral pH value conditions. The WPI absorbance behavior did not change over pH value range of 6.0–7.0, because of the negative net charge of WPI at this pH value range, resulting in electrostatic repulsion in the solution. Further lowering the pH value led to an increase in absorbance, and the maximum turbidity was observed at pH 4.5 (corresponding to the pI of WPI). At pH values lower than the pI of WPI, the aggregation intensity decreased with a decrease in absorbance. Similar results have been reported for basil seed gum-WPI [29], pea protein isolate-high methoxyl pectin [5], and pea protein isolate-pectin [42].

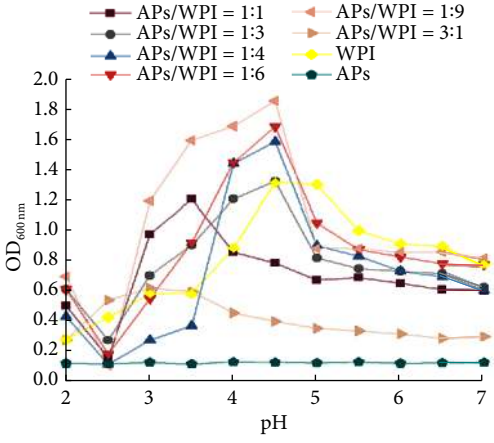


Figure 2 Effect of APs to WPI ratio (*m*/*m*) on turbidity of APs-WPI complex system over pH 2.0–7.0 at 25 °C.

The binary solution of APs-WPI at a mixing ratio of 1:9 (*m*/*m*) showed a different pH-dependent absorbance mode compared with the corresponding individual solutions, where the turbidity increased in two steps, revealing three distinct pH points on the curve. The turbidity remained almost unchanged over pH 7.0 to approximately 6.5, while the turbidity increased slightly after further decrease of the solution's pH value. Therefore, pH 6.5 was designated pH_c in this study, which was indicative of the beginning of soluble complex formation between WPI and APs. The absorbance value increased rapidly when the pH value was lower than 6.5 due to the aggregation of complexes, leading to the formation of particles that showed phase separation. The maximum absorbance of the APs-WPI solution was observed at pH_{opt} = 4.5. The turbidity decreased rapidly when pH value decreased from 4.5 to 3.5 and then showed a gradual reduction with a further pH value decrease. The abrupt decrease in turbidity below pH_{opt} could be attributed to the solubilization of complexes and aggregates due to hydrophobic interactions and hydrogen bonding between components, indicating that lower pH value promoted the interactions between N–H, C–O, or COO– groups in WPI and the hydroxyl groups of APs through hydrogen bonding and molecular hydrophobic effects. Previous studies have reported similar results for soy protein and *β*-glucan [43].

A slight increase in turbidity was observed at pH 2.0, suggesting that the solution of APs-WPI enhanced miscibility. β-Lg is a dimer at neutral pH value, and as the pH value decreases, the structure shifts to the monomer form, which eventually predominates at pH 2.0 [44]. Furthermore, whey proteins carry a net positive charge at pH 2.0, and at low pH values, weak local dipoles of carbohydrate residues may be formed in the APs chain. Compatibility enhancement of weakly charged polyelectrolytes as well as protein-neutral polysaccharide systems has been previously investigated, suggesting that weak biopolymer interactions enhance miscibility [45].

The formation of these large complexes explained the aggregation behaviors of WPI and APs. APs molecules could provide binding sites available for the interaction with WPI. WPI molecules adsorbed on the surface of APs became accessible to APs molecules, resulting in the formation of some local protein domains. These local protein domains could act as joints between WPI-APs complexes, leading to the formation of larger interpolymer complexes with higher turbidity via polymer chain entanglements. In fact, protein association or aggregation can be described as a surface-induced process involving a nucleation step [46]. Changes in pH value that induce protein conformational and compositional changes, modification of intermolecular interactions and increased polysaccharide solubility are expected to influence the flow behavior of the system [45].

Changes in the biopolymer ratio can also affect protein-polysaccharide complex formation, further shifting the critical phase transition boundary pH values [47]. Therefore, the formation of complexes in the APs-WPI as a function of mixing ratio (3:1, 1:1, 1:3, 1:4, 1:6, and 1:9, *m*/*m*) was also investigated through turbidimetry analysis (Figure 2). pH_c remained constant at all biopolymer mixing ratios, while pH_{opt} shifted to lower values with the decrease of WPI ratio. This trend has also been reported previously by other researchers [5, 29, 48]. Soluble complex formation at pH_c is a transition at the molecular level and is not affected by the mixing ratio and the total macromolecular concentration [31]. When the mixing ratio of APs/WPI greater than 1:4, the turbidity increased within a narrow range, suggesting that the number of APs chains was in an excessive state. A similar phenomenon was reported for ovalbumin-XG and lysozyme-XG [49]. In addition, the increasing ratio of APs/WPI from 1:9 to 3:1 favors the formation of the APs-WPI complex due to the lower amounts of WPI molecules in the APs-WPI complexes at a higher mixing ratio. Therefore, the amount of WPI molecules available per APs chain played an important role in the formation of the complexes. The most stable complexes formed at a ratio of 1:9 (APs/WPI) for the binding site reached maximum saturation. These results were also confirmed by the appearance of the APs-WPI complexes as a function of ratio as shown in Figure 3. Phase separation occurred around the plateau pH value. The mechanism of phase separation could be attributed to thermodynamic incompatibility, caused by the excluded volume effect, rather than depletion flocculation [50].

3.2 Effects of pH value and the APs/WPI ratio on the secondary structure of WPI

Table 2 listed the secondary structure content of different APs-WPI complexes at pH_{opt}. A decrease in α-helix contents was found at

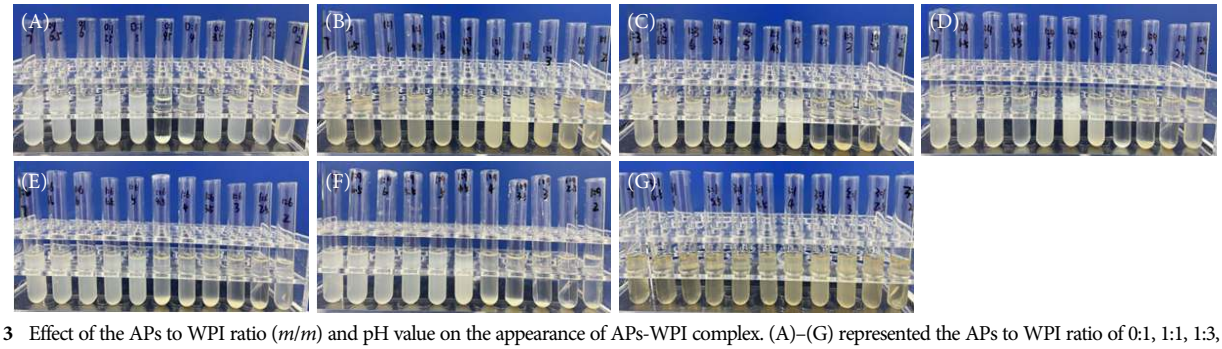


Figure 3 Effect of the APs to WPI ratio (*m*/*m*) and pH value on the appearance of APs-WPI complex. (A)–(G) represented the APs to WPI ratio of 0:1, 1:1, 1:3, 1:4, 1:6, 1:9, and 3:1, respectively. The solution pH value was from 7.0 to 2.0 in a 0.5 stepwise from the left to the right.

Table 2 Composition of the secondary structure of WPI and different ratio of APs-WPI.

pH	Sample	α-Helix		β-Sheet		β-Turn		Random coil	
		Content (%)	Percentage of change (%)	Content (%)	Percentage of change (%)	Content (%)	Percentage of change (%)	Content (%)	Percentage of change (%)
4.5	WPI	14.10		34.20		23.40		31.50	
	APs/WPI = 1:3	12.10	−14.18	32.80	−4.09	23.20	−0.85	31.90	1.27
	APs/WPI = 1:4	13.20	−6.38	31.80	−7.02	22.90	−2.14	32.20	2.22
	APs/WPI = 1:6	13.40	−4.96	31.50	−7.89	23.20	−0.85	31.90	1.27
	APs/WPI = 1:9	12.70	−9.90	31.40	−8.19	22.30	−4.70	32.10	1.59
4.0	WPI	13.30		30.90		23.80		31.90	
	APs/WPI = 1:1	9.90	−25.56	34.80	3.64	23.30	−2.10	32.00	3.13
3.0	WPI	14.10		31.00		23.40		31.50	
	APs/WPI = 1:3	7.60	−46.01	37.00	19.35	23.00	−1.71	32.40	2.86

rates of 14.18%, 6.38%, 4.96%, 9.90%, 25.56%, and 46.01% in the APs-WPI samples of 1:3, 1:4, 1:6, 1:9, 1:1, and 3:1 (APs/WPI), respectively. The β-sheet contents were also decreased for APs/WPI less than 1 (1:3, 1:4, 1:6, 1:9) at rates of 4.09%, 7.02%, 7.89%, and 8.19%, respectively. However, the increases observed in the β-sheet content were 3.64% and 19.35% for ratios of 3:1 and 1:1, respectively. The increase in β-sheet contributed to the exposure of the hydrophobic region of the protein, indicating that the addition of polysaccharides exposes the hydrophobic group of the protein and increases hydrophobicity significantly [51]. Meanwhile, the decreases observed in β-turn contents were 0.85% (1:3), 2.14% (1:4), 0.85% (1:6), 4.70% (1:9), 2.10% (1:1), and 1.71% (3:1), respectively. However, the observed random coil contents were 1.27% (1:3), 2.22% (1:4), 1.27% (1:6), 1.59% (1:9), 3.13% (1:1), and 2.86% (3:1), respectively, indicating partial molecular unfolding and refolding progress when the addition of APs significantly disrupted the α-helix of WPI and increased its flexibility [10]. Table 2 summarized contents of α-helix, β-sheet, β-turn, and random coil in the WPI secondary structure at pH_c. Compared with pH_{opt}, decreased α-helix and β-sheet contents were found. However, the increment β-turn and random coil contents increased in pH_c. In the structure of proteins, β-sheet and β-turn structures are associated with hydrogen bonds [52]. Therefore, it could be hypothesized that the interaction between APs and WPI may be affected by pH value by breaking or forming hydrogen bonds.

The secondary structural changes of proteins can also be monitored by FTIR spectroscopy, which is complementary to CD spectroscopy. As shown in Figures 4(A) and 4(B), two characteristic absorptions of polysaccharides at 3 200–3 600 cm^{-1} and 2 800–3 000 cm^{-1} were due to the stretching vibration of single bond –OH and C–H. The absorption at 1 700–1 750 cm^{-1} was the special absorption of uronic acid. The FTIR spectra of the APs samples exhibited an absorption peak at 890 cm^{-1}, which was the characteristic peak of the β-glucan configuration [23]. However, the absorption at 890 cm^{-1} was not detected for APs-WPI complex, presumably due to the binding of β-glycosidic bonds to WPI. A specific band in the 1 200–1 000 cm^{-1} region was attributed to the ring vibrations overlapped with stretching vibrations of C–OH side groups and the C–O–C glycosidic band vibration. The absorptions at 1 145, 1 075, and 1 042 cm^{-1} indicated a pyranose form of sugar [53]. The amide Ⅰ and Ⅱ bands of WP showed typical bands at 1 641, 1 546, and 1 385 cm^{-1} correspond to amide Ⅰ (C double bond O stretching, 1 600–1 700 cm^{-1} region), amide Ⅱ (N single bond H bending, 1 480–1 600 cm^{-1} region), and C single bond H and C single bond N bending, respectively, which are representative of protein secondary structure involving hydrogen bonding [54]. When the ratio of APs/WPI was 1:9, the amide I peaks of different APs/WPI ratios were observed at 1 649.88 cm^{-1} (APs/WPI = 1:9), 1 650.40 cm^{-1} (APs/WPI = 1:1), and 1 654.28 cm^{-1} (APs/WPI = 3:1) at pH 6.0. The amide I peaks of WPI-APs samples shifted toward higher wavenumbers after the interaction with APs, suggesting that the ratio of APs/WPI affected the structure of complexes. The amide Ⅱ peaks shifted from 1 548.48 cm^{-1} (APs/WPI = 1:1) toward 1 544.18 cm^{-1} (APs/WPI = 1:9) at pH_c, suggesting that APs interacted with WPI via hydrophobic interactions to change the secondary structure of WPI [55]. The amide A peaks (3 000–3 600 cm^{-1}) changed in wavenumber and intensity, suggesting that the introduction of APs could also contribute to an increase in the hydrogen bonding of complex complexes [56]. This result was consistent with other studies on the complex coacervation of chia seed protein isolate-chia seed gum [57], lactoferrin-sodium alginate [40], and pea protein isolate-beet pectin solution [47]. Furthermore, environmental pH value imposed slight peak shifts on the complex coacervate. Compared to that of APs/WPI (1:9), the amide I peak at 1 654.22 cm^{-1} (pH 4.5) shifted to 1 649.88 cm^{-1} (pH 6.0). These results indicated that the overall intermolecular interaction might be affected by environmental pH value conditions [58]. However, the content of β-turns in WPI secondary structure plays an important role in maintaining hydrogen bonds between polyphenol and WPI and the forces between polyphenol and WPI were both hydrogen bonds and van der Waals forces [59, 60]. Therefore, it is hypothesized that the changes in protein secondary structure and hydrogen bond formation may be partly contributed by the polyphenols in APs.

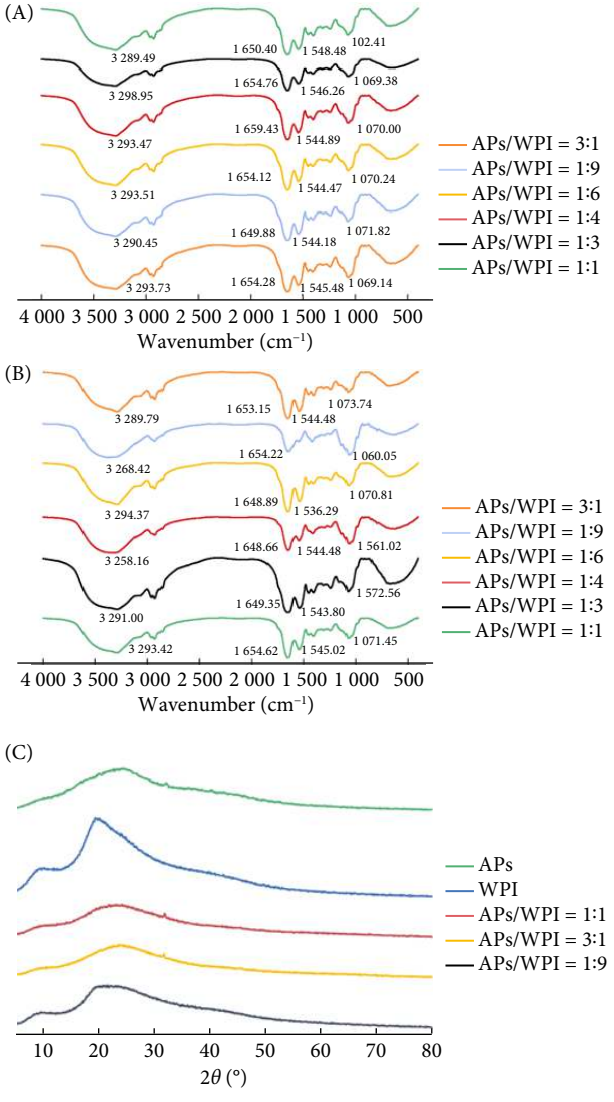


Figure 4 FTIR spectra of APs-WPI solution on at (A) pH_c and (B) pH_{opt}. (C) The XRD spectra of the WPI, APs, and APs-WPI (1:1, 3:1, and 1:9, respectively) at pH_{opt}.

Figure 4(C) showed the diffractograms of different ratios of the APs-WPI complex at pH_{opt} and its individual components, showing

that the structures of both biopolymers were basically amorphous. However, two broad peaks observed in WPI indicated the presence of crystalline regions and noncovalent bonds [32]. The APs-WPI complex presented two refraction peaks similar to those of WPI, suggesting that the APs-WPI complexes retained the amorphous packaging properties of pure WPI [61]. Notably, the intensities of the peaks were different for different ratios of the APs-WPI complexes. The increased APs ratio caused decreased refraction strength because APs were amorphous, thus leading to a decrease in the crystallinity of the complex. Similar results were also found for *Flammulina velutipes* polysaccharides (FVPs)/WPI and epigallocatechin-3-gallate (EGCG)/soy whey wastewater (SWW) [30, 62].

3.3 Size distribution and morphology

The average particle size of complexes in aqueous solution was measured to monitor protein-polysaccharide complex formation and microstructural change of complexes. The particle size distributions of the various ratios of protein-polysaccharide complexes at pH_{opt} are shown in Figure 5. With the increase in the APs ratio, the particle size of the APs-WPI decreased significantly. The particle size of WPI was (5.583 ± 0.401) μm at pH 4.5, while the size of the complex (APs/WPI ratio of 1:9) decreased to (0.417 ± 0.020) μm at pH 4.5. Furthermore, the largest particle sizes were observed for the APs-WPI complexes obtained with an APs/WPI ratio of 3:1, with particle sizes in the APs/WPI and WPI complex solutions of approximately (4.867 ± 0.252) and (2.630 ± 0.252) μm at pH_{opt} (pH = 3), respectively.

AFM was used to further characterize the morphology of the APs-WPI complexes at different pH_{opt} values. It was directly observed the extended stiff chain conformation by AFM. For lyophilized droplets of WPI solution, the structural surface was relatively intact, while the internal particles mainly exhibit spherical structures. As presented in Figure 6, the surfaces of the APs-WPI complexes (3:1, *m*/*m*) under pH_{opt} were irregular schistose, rounded edges, and tight and compact network-like structures at pH 3.0. When the APs ratio increased, most polysaccharide chains primarily turned and assembled to form string-like nanofibers and tended to form a continuous phase, such as thin film or lamella [35]. Moreover, the network was clearly observed as the APs fraction incorporated into the gel formulation increased. This result suggested that the gel network might arise from the APs chains. A similar phenomenon was found for XG and *β*-Lg and for peanut polysaccharide (PPS) and co-dissolution of residual protein from byproduct (PPSI) [8, 63]. A reasonable explanation was that the high polysaccharide ratio was favorable for the formation of a stable biopolymer web to encapsulate protein, and consequently, the aggregated molecules could not form precipitation.

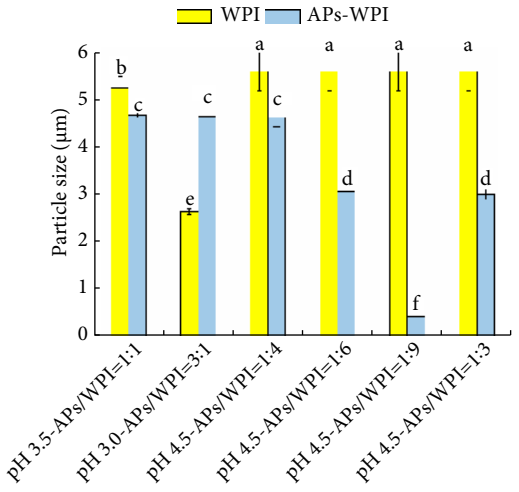


Figure 5 Changes in the particle size of WPI and APs-WPI solution at pH_{opt}. The different letters mean significance differences between different groups ($P < 0.05$).

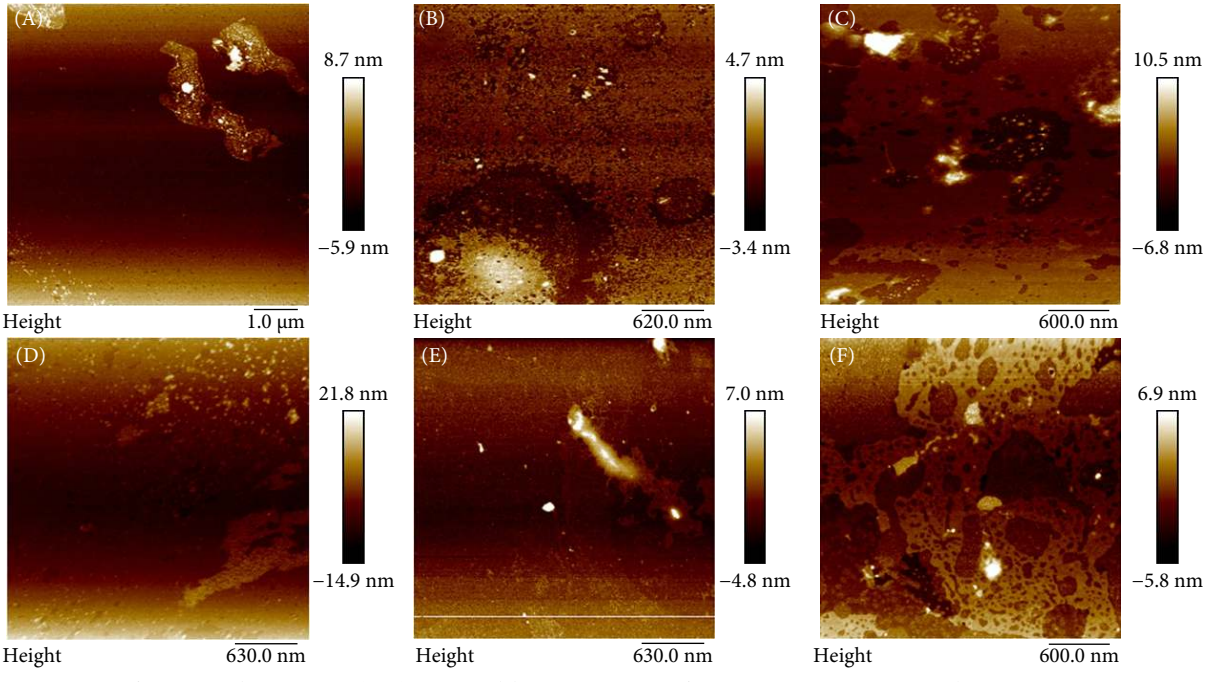


Figure 6 AFM images of APs-WPI solution at pH_{opt}. (A–F) represented the APs to WPI ratio of 1:1, 1:3, 1:4, 1:6, 1:9, 3:1, respectively.

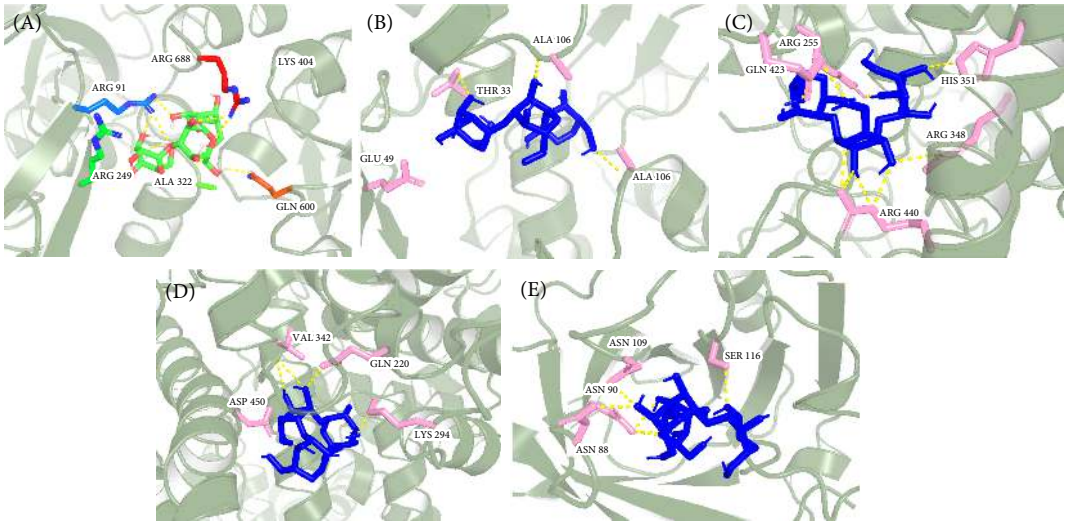


Figure 7 The binding mode of β-glucan and the (A) β-Lg, (B) α-La, (C) lactoferrin, (D) lactoperoxidase, and (E) BSA. The cyclodextrins are presented as blue sticks, and the amino acid residues related to cyclodextrin binding are presented as pink sticks.

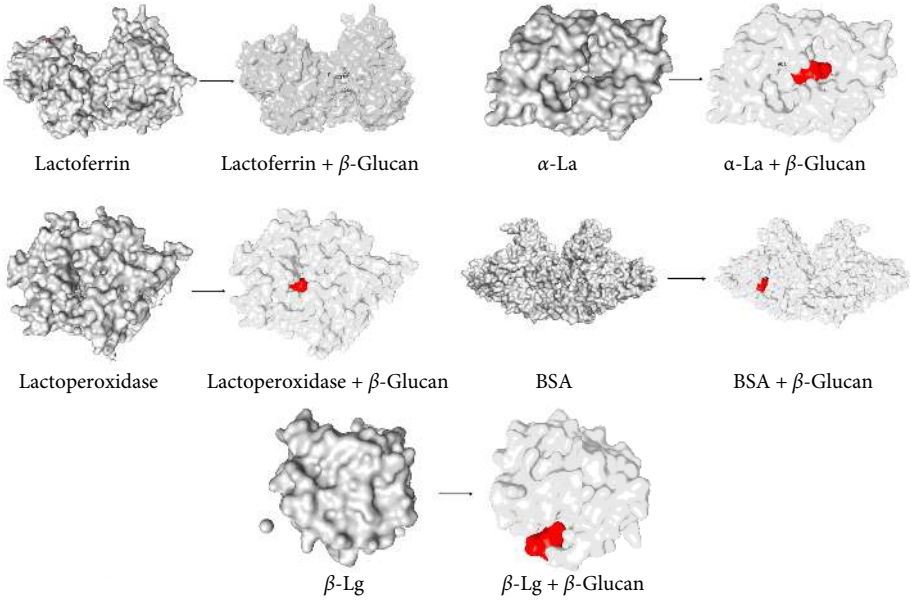


Figure 8 Model diagram of protein conformational change, red is polysaccharide binding.

3.4 Analysis of binding sites between β-glucan and WPI

The binding process between the amino acid residues of WPI and β-glucan in APs was obtained by molecular docking analysis. The binding energy between β-Lg, α-La, lactoperoxidase, lactoferrin, BSA, and β-glucan is −6.4, −8.3, −8.7, −8.9, and −7.8 kcal/mol, respectively. As shown in Figure 7(A), β-Lg interacted with APs through hydrogen bonds (Asn 109, Asn 90, Asn 88, and Ser 116), while APs interacted with α-La through Glu 49 (van der Waals force), Thr 33 (hydrogen bond) and Ala 106 (hydrogen bond). As shown in Figure 7(B), the amino acid residues in lactoferrin related to APs binding were Gln 600 (hydrogen bond), Arg 688 (hydrogen bond), Arg 91 (hydrogen bond), Arg 249 (hydrogen bond), Ala 322 (hydrogen bond), and Lys 404 (van der Waals force) (Figure 7(C)). APs interacted with lactoperoxidase through hydrogen bonds (Arg 255, Gln 423, Arg 400, ARG 248, and His 351), as shown in Figure 7(D), while APs interacted with BSA through hydrogen bonds (Val 342, Gln 220, and Lys 294) and hydrophobic interactions (Asp 450) (Figure 7(E)). APs interacted with WPI mainly through noncovalent binding, changing the structure of WPI (Figure 8). These hydrogen bonds enhanced the strength of noncovalent bonding during the interaction process and stabilized the spatial conformation of the β-glucan and β-glucan-WPI complex [37]. Furthermore, van der Waals forces between the β-glucan and WPI residues significantly supported the spatial conformation of the complex. Cyclodextrins interacted with pullulanase through hydrogen bonds, van der Waals forces and hydrophobic interactions. Phenylalanine 476 is the key amino acid residue in pullulanase for cyclodextrin recognition and binding [36]. Similar results were reported in which the –OH and –COOH groups of sodium alginate formed hydrogen bonds with amino acid residues of β-Lg [40, 64].

4 Conclusion

This study showed the compounding behavior of APs and WPI

under different conditions (pH value and mixing ratio) via noncovalent interactions. The results confirmed that APs could interact with WPI via hydrogen bonding and hydrophobic interactions. The turbidity profiles revealed that the interaction behavior was affected by the pH value and mixing ratio of WPI-APs. As the mass ratio of WPI to APs increased, the critical pH value of the complex shifted toward higher values, as more WPI molecules were available for binding to the APs chains. The interactions between APs and WPI might also be pH-dependent via breaking or forming hydrogen bonds. The FTIR, CD, and XRD results showed the differences in secondary structures and conformation between APs-WPI and WPI. Of note from the current study, the optimization of pH value and mixing ratio of protein-polysaccharide complexation were the prerequisites for the desired microstructure and stability properties of the compound solutions. Further work will be done in the application of APs-WPI complexes in the area of acidified emulsions.

Conflict of interest

The authors declare no conflict of interest.

Acknowledgments

This study was funded by the Heilongjiang Province Natural Science Foundation of China (Nos. LH2021C075 and LH2022C075).

References

[1] L. Gentile, Protein-polysaccharide interactions and aggregates in food formulations, Curr. Opin. Colloid. In. 48 (2020) 18–27. https://doi.org/10.1016/j.cocis.2020.03.002.

[2] N. Nayak , H. Singh, Milk protein-polysaccharide interactions in food systems, in: Encyclopedia of food chemistry, Elsevier, 2018, pp. 431–438.

[3] J. Carpentier, E. Conforto, C. Chaigneau, et al., Complex coacervation of pea protein isolate and tragacanth gum: comparative study with commercial polysaccharides, Innov. Food Sci. Emerg. 69 (2021). https://doi.org/10.1016/j.ifset.2021.102641.

[4] E. Dickinson, Biopolymer-based particles as stabilizing agents for emulsions and foams, Food Hydrocoll. 68 (2017) 219–231. https://doi.org/10.1016/j.foodhyd.2016.06.024.

[5] Y. Lan, B. Chen, J. Rao, Pea protein isolate-high methoxyl pectin soluble complexes for improving pea protein functionality: effect of pH, biopolymer ratio and concentrations, Food Hydrocoll. 80 (2018) 245–253. https://doi.org/10.1016/j.foodhyd.2018.02.021.

[6] S. S. N. Chakravartula, M. Soccio, N. Lotti, et al., Characterization of composite edible films based on pectin/alginate/whey protein concentrate, Materials 12 (2019) 2454. https://doi.org/10.3390/ma12152454.

[7] F. Alavi, L. Chen, Complexation of nanofibrillated egg white protein and low methoxy pectin improves microstructure, stability, and rheology of oil-in-water emulsions, Food Hydrocoll. 124 (2022). https://doi.org/10.1016/j.foodhyd.2021.107262.

[8] J. Ye, X. Hua, W. Zhang, et al., Emulsifying capacity of peanut polysaccharide: improving interfacial property through the co-dissolution of protein during extraction, Carbohydr. Polym. 273 (2021). https://doi.org/10.1016/j.carbpol.2021.118614.

[9] J. Cheng, Y. Ma, X. Li, Effects of milk protein-polysaccharide interactions on the stability of ice cream mix model systems, Food Hydrocoll. 45 (2015) 327–336. https://doi.org/10.1016/j.foodhyd.2014.11.027.

[10] W. Chen, W. Wang, X. Ma, et al., Effect of pH-shifting treatment on structural and functional properties of whey protein isolate and its interaction with (–)-epigallocatechin-3-gallate, Food Chem. 274 (2019) 234–241. https://doi.org/10.1016/j.foodchem.2018.08.106.

[11] B. G. Carter, E. A. Foegeding, M. A. Drake, Invited review: astringency in whey protein beverages, J. Dairy Sci. 103 (2020) 5793–5804. https://doi.org/10.3168/jds.2020-18303.

[12] J. Hu, T. F. Zhao, S. J. Li, Stability, microstructure, and digestibility of whey protein isolate-*Tremella fuciformis* polysaccharide complexes, Food Hydrocoll. 89 (2019) 379–385. https://doi.org/10.1016/j.foodhyd.2018.11.005.

[13] Z. Jiang, Y. Gao, J. Li, et al., Consecutive pH-shift and ultrasound treatment modify the physicochemical properties of whey protein isolate, Int. Dairy J. 127 (2022) 105211. https://doi.org/10.1016/j.idairyj.2021.105211.

[14] F. Cui, D. J. McClements, X. Liu, et al., Development of pH-responsive emulsions stabilized by whey protein fibrils, Food Hydrocoll. 122 (2022) 107067. https://doi.org/10.1016/j.foodhyd.2021.107067.

[15] X. Du, X. Huang, L. Wang, et al., Nanosized niosomes as effective delivery device to improve the stability and bioaccessibility of goat milk whey protein peptide, Food Res. Int. 161 (2022) 111729. https://doi.org/10.1016/j.foodres.2022.111729.

[16] J. Aschemann-Witzel, P. Varela, A. Peschel, Consumers' categorization of food ingredients: do consumers perceive them as 'clean label' producers expect? An exploration with projective mapping, Food Qual. Prefer. 71 (2019) 117–128. https://doi.org/10.1016/j.foodqual.2018.06.003.

[17] M. Sarraf, S. Naji-Tabasi, A. Beig-Babaei, Influence of calcium chloride and pH on soluble complex of whey protein-basil seed gum and xanthan gum, Food Sci. Nutr. 9 (2021) 6728–6736. https://doi.org/10.1002/fsn3.2624.

[18] W. Wijaya, S. Turan, A. Diah, et al., Effect of low-methoxy pectin on interfacial and emulsion stabilizing properties of heated whey protein isolate (WPI) aggregates, Food Struct. 26 (2020) 100159. https://doi.org/10.1016/j.foostr.2020.100159.

[19] Wusigale, L. Liang, Y. C. Luo, Casein and pectin: structures, interactions, and applications, Trends Food Sci. Tech. 97 (2020) 391–403. https://doi.org/10.1016/j.tifs.2020.01.027..

[20] F. Du, Y. Qi, H. Huang, et al., Stabilization of o/w emulsions via interfacial protein concentrating induced by thermodynamic incompatibility between sarcoplasmic proteins and xanthan gum, Food Hydrocoll. 124 (2022). https://doi.org/10.1016/j.foodhyd.2021.107242.

[21] D. Liu, P. Zhou, T. Nicolai, Effect of kappa carrageenan on acid-induced gelation of whey protein aggregates. Part I: potentiometric titration, rheology and turbidity, Food Hydrocoll. 102 (2020). https://doi.org/10.1016/j.foodhyd.2019.105589.

[22] J. Miao, J. M. Regenstein, J. Qiu, et al., Isolation, structural characterization and bioactivities of polysaccharides and its derivatives from *Auricularia*: a review, Int. J. Biol. Macromol. 150 (2020) 102–113. https://doi.org/10.1016/j.ijbiomac.2020.02.054.

[23] S. Xu, X. Xu, L. Zhang, Branching structure and chain conformation of water-soluble glucan extracted from *Auricularia auricula-judae*, J. Agric. Food Chem. 60 (2012) 3498–3506. https://doi.org/10.1021/jf300423z.

[24] P. Shao, J. Feng, P. Sun, et al., Recent advances in improving stability of food emulsion by plant polysaccharides, Food Res Int. 137 (2020) 109376. https://doi.org/10.1016/j.foodres.2020.109376.

[25] N. Chen, H. Zhang, X. Zong, et al., Polysaccharides from *Auricularia auricula*: preparation, structural features and biological activities, Carbohydr. Polym. 247 (2020) 116750. https://doi.org/10.1016/j.carbpol.2020.116750.

[26] H. Bao, S. You, L. Cao, et al., Chemical and rheological properties of polysaccharides from fruit body of *Auricularia auricular-judae*, Food Hydrocoll. 57 (2016) 30–37. https://doi.org/10.1016/j.foodhyd.2015.12.031.

[27] Y. Zhao, D. Shui, S. Li, et al., Complexation behavior of *Auricularia* auriculapolysaccharide and whey protein isolate: characterization and potential beverage application, J. Food Process Pres. 46 (2022) e16340. https://doi.org/10.1111/jfpp.16340.

[28] J. Shang, J. Ritian, W. Yang, et al., The effect of different edible fungal polysaccharides on the stability of whey protein isolate solution near isoelectric point, Int. J. Food Sci. Tech. (2023) 16259. https://doi.org/10.1111/ijfs.16259.

[29] B. Fataneh, M. A. R. Seyed, H. Joyner, Mechanisms of whey protein isolate interaction with basil seed gum: influence of pH and protein-polysaccharide ratio, Carbohydr. Polym. 232 (2020) 115775. https://doi.org/10.1016/j.carbpol.2019.115775.

[30] J. Shang, M. Liao, R. Jin, et al., Molecular properties of *Flammulina velutipes* polysaccharide-whey protein isolate (WPI) complexes via noncovalent interactions, Foods 10 (2020) 1. https://doi.org/10.3390/foods10010001.

[31] H. Li, T. Wang, Y. Hu, et al., Designing delivery systems for functional ingredients by protein/polysaccharide interactions, Trends Food Sci. Technol. 119 (2022) 272–287. https://doi.org/10.1016/j.tifs.2021.12.007.

[32] D. A. González-Martínez, H. Carrillo-Navas, C. E. Barrera-Díaz, et al., Characterization of a novel complex coacervate based on whey protein isolate-tamarind seed mucilage, Food Hydrocoll. 72 (2017) 115–126. https://doi.org/10.1016/j.foodhyd.2017.05.037.

[33] J. Wang, S. Nie, Application of atomic force microscopy in microscopic analysis of polysaccharide, Trends Food Sci. Technol. 87 (2019) 35–46. https://doi.org/10.1016/j.tifs.2018.02.005.

[34] X. Li, Y. Bai, H. Ji, et al., The binding mechanism between cyclodextrins and pullulanase: a molecular docking, isothermal titration calorimetry, circular dichroism and fluorescence study, Food Chem. 321 (2020) 126750. https://doi.org/10.1016/j.foodchem.2020.126750.

[35] Y. Lv, Q. Liang, Y. Li, et al., Study of the binding mechanism between hydroxytyrosol and bovine serum albumin using multispectral and molecular docking, Food Hydrocoll. 122 (2022) 107072. https://doi.org/10.1016/j.foodhyd.2021.107072.

[36] T. Dai, R. Li, C. Liu, et al., Effect of rice glutelin-resveratrol interactions on the formation and stability of emulsions: a multiphotonic spectroscopy and molecular docking study, Food Hydrocoll. 97 (2019) 105234. https://doi.org/10.1016/j.foodhyd.2019.105234.

[37] Y. Xu, M. Shen, Y. Chen, et al., Optimization of the polysaccharide hydrolysate from *Auricularia auricula* with antioxidant activity by response surface methodology, Int. J. Biol. Macromol. 113 (2018) 543–549. https://doi.org/10.1016/j.ijbiomac.2018.02.059.

[38] S. Cao, X. He, L. Qin, et al., Anticoagulant and antithrombotic properties *in vitro* and *in vivo* of a novel sulfated polysaccharide from marine green alga *Monostroma nitidum*, Mar. Drugs 17 (2019). https://doi.org/10.3390/md17040247.

[39] R. Sánchez, C. Juan, J. Benavides, et al., The folin-ciocalteu assay revisited: improvement of its specificity for total phenolic content determination, Anal. Methods. 5 (2013) 5990–5999. https://doi.org/10.1039/C3AY41125G.

[40] L. P. H. Bastos, C. W. P. de Carvalho, E. E. Garcia-Rojas, Formation and characterization of the complex coacervates obtained between lactoferrin and sodium alginate, Int. J. Biol. Macromol. 120 (2018) 332–338. https://doi.org/10.1016/j.ijbiomac.2018.08.050.

[41] T. Wagoner, B. Vardhanabhuti, E. A. Foegeding, Designing whey protein-polysaccharide particles for colloidal stability, Annu. Rev. Food Sci. Technol. 7 (2016) 93–116. https://doi.org/10.1146/annurev-food-041715-033315.

[42] Y. Lan, J. B. Ohm, B. Chen, et al., Phase behavior, thermodynamic and microstructure of concentrated pea protein isolate-pectin mixture: effect of pH, biopolymer ratio and pectin charge density, Food Hydrocoll. 101 (2020) 105556. https://doi.org/10.1016/j.foodhyd.2019.105556.

[43] R. L. Shen, X. Y. Liu, J. L. Dong, et al., The gel properties and microstructure of the mixture of oat β-glucan/soy protein isolates, Food Hydrocoll. 47 (2015) 108–114. https://doi.org/10.1016/j.foodhyd.2015.01.017.

[44] C. C. Chen, S. T. Chen, J. F. Hsieh, Proteomic analysis of polysaccharide-milk protein interactions induced by chitosan, Molecules 20 (2015) 7737–7749. https://doi.org/10.3390/molecules20057737.

[45] V. Kontogiorgos, S. M. Tosh, P. J. Wood, Phase behaviour of high molecular weight oat β-glucan/whey protein isolate binary mixtures, Food Hydrocoll. 23 (2009) 949–956. https://doi.org/10.1016/j.foodhyd.2008.07.005.

[46] M. Rabe, D. Verdes, S. Seeger, Understanding protein adsorption phenomena at solid surfaces, Adv. Colloid. Interface Sci. 162 (2011) 87–106. https://doi.org/10.1016/j.cis.2010.12.007.

[47] Y. Lan, J. B. Ohm, B. Chen, Phase behavior and complex coacervation of concentrated pea protein isolate-beet pectin solution, Food Chem. 307 (2020) 125536. https://doi.org/10.1016/j.foodchem.2019.125536.

[48] K. Hoda, E. Bahareh, K. Rassoul, et al., Effects of biopolymer ratio and heat treatment on the complex formation between whey protein isolate and soluble fraction of persian gum, J. Dispers. Sci. Technol. 38 (2017) 1234–1241. https://doi.org/10.1080/01932691.2016.1230064.

[49] C. J. F. Souza, E. E. Garcia-Rojas, Effects of salt and protein concentrations on the association and dissociation of ovalbumin-pectin complexes, Food Hydrocoll. 47 (2015) 124–129. https://doi.org/10.1016/j.foodhyd.2015.01.010.

[50] J. Liu, J. Chai, T. Zhang, et al., Phase behavior, thermodynamic and rheological properties of ovalbumin/dextran sulfate: effect of biopolymer ratio and salt concentration, Food Hydrocoll. 118 (2021) 106777. https://doi.org/10.1016/j.foodhyd.2021.106777.

[51] R. Zhang, X. Pang, J. Lu, Effect of high intensity ultrasound pretreatment on functional and structural properties of micellar casein concentrates, Ultrason. Sonochem. 47 (2018) 10–16. https://doi.org/10.1016/j.ultsonch.2018.04.011.

[52] Q. Li, Z. Wang, C. Dai, Physical stability and microstructure of rapeseed protein isolate/gum arabic stabilized emulsions at alkaline pH, Food Hydrocoll. 88 (2019) 50–57. https://doi.org/10.1016/j.foodhyd.2018.09.020.

[53] W. C. Zeng, Z. Zhang, H. Gao, et al., Characterization of antioxidant polysaccharides from *Auricularia auricular* using microwave-assisted extraction, Carbohydr. Polym. 89 (2012) 694–700. https://doi.org/10.1016/j.carbpol.2012.03.078.

[54] H. Wang, L. Ke, J. Zhou, et al., Multi-spectroscopic, molecular docking and molecular dynamic simulation evaluation of hydroxychloroquine sulfate interaction with caseins and whey proteins, J. Mol. Liq. 367 (2022). https://doi.org/10.1016/j.molliq.2022.120460.

[55] P. Guerrero, J. P. Kerry, K. de la Caba, FTIR characterization of protein-polysaccharide interactions in extruded blends, Carbohydr. Polym. 111 (2014) 598–605. https://doi.org/10.1016/j.carbpol.2014.05.005.

[56] Y. G. Zhao, N. Khalid, G. F. Shu, et al., Complex coacervates from gelatin and octenyl succinic anhydride modified kudzu starch: insights of formulation and characterization, Food Hydrocoll. 86 (2019) 70–77. https://doi.org/10.1016/j.foodhyd.2018.01.040.

[57] Y. P. Timilsena, B. Wang, R. Adhikari, et al., Preparation and characterization of chia seed protein isolate-chia seed gum complex coacervates, Food Hydrocoll. 52 (2016) 554–563. https://doi.org/10.1016/j.foodhyd.2015.07.033.

[58] Y. Li, X. Zhang, Y. Zhao, et al., Investigation on complex coacervation between fish skin gelatin from cold-water fish and gum arabic: phase behavior, thermodynamic, and structural properties, Food Res. Int. 107 (2018) 596–604. https://doi.org/10.1016/j.foodres.2018.02.053.

[59] Y. Wang, J. Zhang, L. F. Zhang, Study on the mechanism of non-covalent interaction between rose anthocyanin extracts and whey protein isolate under different pH conditions, Food Chem. 384 (2022) 132492. https://doi.org/10.1016/j.foodchem.2022.132492.

[60] T. Zhao, B. Yang, S. Ji, et al., Effects of the structure and interaction force of phytosterol/whey protein isolate self-assembly complex on phytosterol digestion properties, Food Chem. 403 (2023) 134311. https://doi.org/10.1016/j.foodchem.2022.13431.

[61] Y. P. Neo, S. Ray, J. Jin, et al., Encapsulation of food grade antioxidant in natural biopolymer by electrospinning technique: a physicochemical study based on zein-gallic acid system, Food Chem. 136 (2013) 1013–1021. https://doi.org/10.1016/j.foodchem.2012.09.010.

[62] Z. Xu, N. Hao, L. Li, et al., Valorization of soy whey wastewater: how epigallocatechin-3-gallate regulates protein precipitation, ACS Sustain. Chem. Eng. 7 (2019) 15504–15513. https://doi.org/10.1021/acssuschemeng.9b03208.

[63] X. T. Le, S. L. Turgeon, Rheological and structural study of electrostatic cross-linked xanthan gum hydrogels induced by *β*-lactoglobulin, Soft Matter 9 (2013) 3063–3073. https://doi.org/10.1039/C3SM27528K.

[64] X. Liu, X. Qin, Y. Wang, et al., Physicochemical properties and formation mechanism of whey protein isolate-sodium alginate complexes: experimental and computational study, Food Hydrocoll. 131 (2022) 107786. https://doi.org/10.1016/j.foodhyd.2022.107786.